Received: April 26, 2022. Revised: June 7, 2022.

INASS

International Journal of
Intelligent Engineering & Systems

http://www.inass.org/

Direct Torque Control for Permanent Magnet Synchronous Motor Using Golden Eagle Optimized ANFIS

Marulasiddappa Hallikeri Basappa[1]* **Pushparajesh Viswanathan[1]**

[1]*Jain (Deemed-to-be University), India*
* Corresponding author's Email: Marul.bethur@gmail.com

Abstract: Nowadays, the Permanent Magnet Synchronous Motors (PMSM) are gaining popularity among electric motors due to their high efficiency, high-speed operation, ruggedness, and small size. PMSM motors comprise a trapezoidal electromotive force which is also called synchronous motors. Direct Torque Control (DTC) has been extensively applied in speed regulation systems due to its better dynamic behaviour. The controller manages the amplitude of torque and stator flux directly using the direct axis current. To manage the motor speed, the torque error, flux error, and projected location of flux linkage are employed to adjust the switching sequence of inverter. One of the most common problems encountered in a PMSM motor is Torque ripple, which is recreated by power electronic commutation and a better controller reduces the ripples to increase the drive's performance. Here, DTC control of PMSM is controlled by Golden Eagle Optimization (GEO) optimized Adaptive Neuro-Fuzzy Inference System (ANFIS). Learning parameters of the ANFIS are optimized for various operating functions by GEO in terms of speed and torque. In this work, simulation results are carried out in MATLAB, it shows that GEO-ANFIS controller is used in conjunction with a PMSM motor to attain less torque ripple up to 0.44 Nm and maintain the speed with a distortion error of 2.12 % when compared with Space Vector Pulse Width Modulation based DTC (SVPWM-DTC) and Dual Cost Function Model Predictive Direct Speed Control (DCF-MPDSC).

Keywords: Adaptive neuro-fuzzy inference system, Direct torque control, Golden eagle optimization, Permanent magnet synchronous motors, Torque ripple.

1. Introduction

For the past few years, PMSM has recently been selected as the driving machine of Electric Vehicles (EV) because of its maximum reliability, high torque intensity and compact volume. It can be assembled into two primary groups: Vector Control (VC) and DTC [1, 2]. Although VC provides good dynamic and steady-state performance, the bandwidth constraint prevents it from being used in high-performance environments [3]. DTC has a high torque response speed, but it also has a significant torque ripple [4]. Many control strategies have been created to address the inadequacies of traditional control approaches. The complicated working environment of electric vehicles exhibits substantial difficulties in the development of control mechanisms. The DTC provides advantages based on the switching voltage table, such as a simple structure and quick torque responses [5]. The following key issues arise as a result of this control strategy: torque ripple, unregulated moving regularity, and susceptibility to resistance fluctuation. Artificial intelligence can help tackle these issues and improve induction machine DTC [6].

Torque is still the most significant control target in an electric vehicle's control system. Many academics have been interested in Model Predictive Torque Control (MPTC) with its rapid torque response and unrestricted synthesis of numerous restrictions [7]. MPTC can predict the machine's behavior in the future and choose the best voltage smear to drive based on the designed cost function [8]. The ideal voltage vector chosen by minimizing the cost function is more precise and efficient than DTC. Other limitations can also be incorporated into the cost function to enhance the system's control

performance [9]. MPTC offers a faster torque response than VC and is, therefore, better suited to applications demanding high torque response. However, MPTC suffers from significant torque ripple and a variable switching frequency [10]. To address this issue, the Duty Cycle Control (DCC) concept of DTC control is applied which significantly reduces torque ripple [11]. The correctness of the model parameters determines the machine behaviors anticipated by the model at the next extreme. Soft computational approaches for intelligent control, including neural networks, neuro-fuzzy and fuzzy logic are well-known and have been used by many researchers in the driving field [12]. This paper [13] establishes a hybrid intelligent controller, which reduces the torque, ripples and improves performance. However, numerous applications have to focus not only on the driving field but also on the maturation of the underlying technology. Till now, so many control approaches were introduced, but, none of these approaches were successful in producing a perfect ripple-free speed and torque [14, 15].

For PMSMs drives, Hybrid Wolf Optimization Algorithm [16] was industrialized to reduce the torque ripple. Conversely, the instability of the procedure was not eliminated. To eliminate torque ripple effectively, hybrid Genetic Algorithm-Gravitational Search Algorithm (HGA-GSA) [17] established on the predetermined mechanism for PMSM drives. For the PMSM drive system, a unique duty ratio modulated direct torque control (DDTC) [18] was presented. The variation rate of d-axis current has no bearing on the torque modifications, whereas the q-axis current variation is proportionate to torque difference. In PMSM, a novel hybrid DTC method [19] was presented, but it produces high current harmonics and flux ripples in all the conditions. To improve the dynamics of torque and flux, a hybrid control technique [20] for PMSM was established, but the switching loss was high. The Space Vector Pulse Width Modulation based DTC (SVPWM-DTC) [21] was suggested for PMSM; due to the bandwidth constraint, it causes a huge torque ripple in the motor. A novel Dual Cost Function Model Predictive Direct Speed Control (DCF-MPDSC) [22] was presented with duty ratio optimization for PMSM drives. Even though several equations are involved, only one voltage vector is applied throughout the control period which resulting in a huge torque ripple. Various control techniques has been proposed for Electric Vehicles in [23].

PMSM drives are suitable for high power density design approach. These motors are the most preferred motors for the electric vehicle application due to its traction characteristics. Adjusting and computing the constraints by means of ordinary PID is problematic and similarly it does not provide fulfilled control features. To overcome those issues, this research displays proposed GEO-ANFIS to regulate torque and motor speed while the load diverges. The main-criteria in the designing and tuning using proposed GEO-ANFIS is the controllability of speed in PMSM without any overshoot with good transient response. Furthermore, it provides a proper and continuous tuning of parameter which refers to an effective model of PMSM drives. The major contribution of this research is mentioned as follows,

- In this research, proposed GEO-ANFIS control is presented to adjust the control parameters under various load conditions to maintain torque and speed.
- To enhance the GEO-ANFIS performance, there is a rise in the membership functions input is required.
- Also, the specific rules are designed for every gain values. With the help of specific rules, the controller adjusting values of constraints.

The organization of this research paper are mentioned as follows; Section 2 represents the explanation for DTC of PMSM along with proposed GEO-ANFIS process. Section 3 stated the result and discussion with comparative analysis of proposed GEO-ANFIS. Lastly, Section 4 declared the conclusion part.

2. Proposed method

In this paper, ANFIS based speed and torque controller is presented for PMSM. GEO is applied for optimizing the learning parameter of ANFIS under various operating modes. The major goal of this research is to improve the PMSM drive's performance by developing a DTC scheme that allows for even more speed control tracking and seamless torque response.

2.1 Direct torque control of PMSM motor

The basic operating principle of the DTC is to select a vector difference between the measured torque, expected torque and flux measurements. The DTC may be able to control speed without the usage of mechanical sensors. DTC is a control method for directly and independently controlling the torque of variable frequency drives. To maintain the torque and flux within hysteresis limitations, the error signals are employed to operate the six switch inverter. Fig. 1 represents the general illustration of the DTC of PMSM using GEO-ANFIS controller.

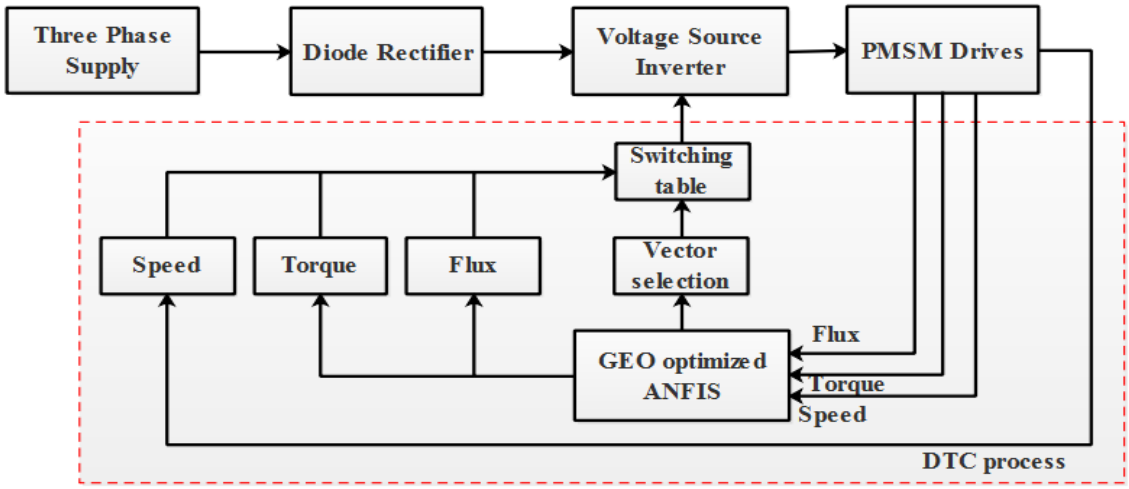

Figure. 1 DTC for PMSM drive

Fig. 2 shows the d-q axes reference frame of PMSM drives. The stator impedances and self-inductance of all primary winding are assumed to be equal in the modelling of the PMSM motor. The stator phase voltage equation of a PMSM motor is identical to the armature formula of DC machines, which can be written in matrix form as shown in Eq. (1).

$$\begin{bmatrix} V_a \\ V_b \\ V_c \end{bmatrix} = R \begin{bmatrix} 1 & 0 & 0 \\ 0 & 1 & 0 \\ 0 & 0 & 1 \end{bmatrix} \begin{bmatrix} i_a \\ i_b \\ i_c \end{bmatrix} + \begin{bmatrix} L-M & 0 & 0 \\ 0 & L-M & 0 \\ 0 & 0 & L-M \end{bmatrix} \frac{d}{dt} \begin{bmatrix} i_a \\ i_b \\ i_c \end{bmatrix} + \begin{bmatrix} E_a \\ E_b \\ E_c \end{bmatrix} \quad (1)$$

Where $V_a, V_b \; and \; V_c$ represents the stator phase voltages, E_a, E_b and E_c are the trapezoidal back emf, i_a, i_b and i_c are the motor input current and R_a, R_b and R_c represents the terminal resistances. The L and M represent the self and mutual inductances respectively. The electromagnetic torque of the PMSM motor can be estimated by Eq. (2).

$$T_e = \frac{P}{w_m} \quad (2)$$

Where,

$$P = E_a i_a + E_b i_b + E_c i_c$$

The electromagnetic torque of the PMSM motor in the synchronously rotating frames can be estimated as Eq. (3).

$$T_e = \frac{3}{2}\frac{p}{2}\left[\left(\frac{dL_d}{d\theta_e} i_{sd} + \frac{d\varphi_{rd}}{d\theta_e} - \varphi_{sq}\right) i_{sd} + \left(\frac{dL_q}{d\theta_e} i_{sq} + \frac{d\varphi_{rq}}{d\theta_e} - \varphi_{sd}\right) i_{sq}\right] \quad (3)$$

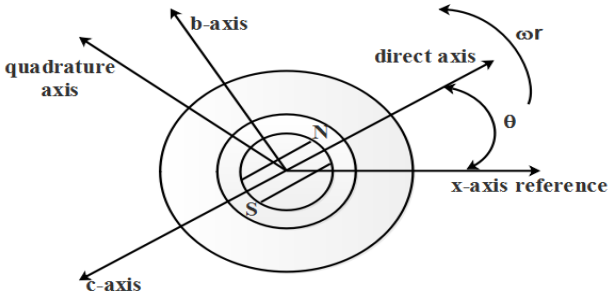

Figure. 2 d-q axes reference for PMSM drive

Where,

$$\varphi_{sq} = L_q i_{sq} + \varphi_{rq}$$

$\varphi_{sd} = L_d i_{sd} + \varphi_{rd}$ and p is the number of poles, i_{sd}, i_{sq}, L_d and L_q represents the d and q axes currents and inductances respectively, θ_r represent the rotor angle and φ_{rd}, φ_{rq}, φ_{sd} and φ_{sq} are the rotor and stator flux linkages in the d and q axes respectively. This electromagnetic torque equation can be simplified by converting it into a stationary $\alpha\beta$ frame, which is written as Eq. (4).

$$T_e = \frac{3}{2}\frac{p}{2}\left[\frac{d\varphi_{r\alpha}}{d\theta_e} i_{s\alpha} + \frac{d\varphi_{r\beta}}{d\theta_e} i_{s\beta}\right] \quad (4)$$

Where $\varphi_{r\alpha}$ and $\varphi_{r\beta}$ are the α and β axes rotor flux linkages. The stator flux linkages are estimated from the measured stationary α-β reference frame stator current and voltage. The stator flux linkage and its vector position are given as in Eqs. (5) to (7).

$$\varphi_{s\alpha} = V_{s\alpha} t - R_s \int i_{s\alpha} dt + \varphi_{s\alpha}(0) \quad (5)$$

$$\varphi_{s\beta} = V_{s\beta} t - R_s \int i_{s\beta} dt + \varphi_{s\beta}(0) \quad (6)$$

$$\theta_s = \tan^{-1} \frac{\varphi_{s\beta}}{\varphi_{s\alpha}} \quad (7)$$

Table 1. Switching table for DTC control

Flux	Torque	Sector					
		1	2	3	4	5	6
1	1	V2	V3	V4	V5	V6	V1
	0	V0	V7	V0	V7	V0	V7
	-1	V6	V1	V2	V3	V4	V5
0	1	V3	V4	V5	V6	V1	V2
	0	V7	V0	V7	V0	V7	V0
	-1	V5	V6	V1	V2	V3	V4

Where $\varphi_{s\alpha}(0)$ and $\varphi_{s\beta}(0)$ are the initial stator flux linkage values, which is given as Eq. (8).

$$\varphi_{s\alpha}(0) = 0$$

$$\varphi_{s\beta}(0) = \frac{2K_b\pi}{3\sqrt{3}} \tag{8}$$

Where K_b is the back emf constant, from the above Eq. (8), flux, torque and sector angle can be estimated.

The calculated flux and torque are associated with the sample standards, and an error signal is generated. The voltage course is selected and inverter switching is controlled based on the errors and sector angle. Table 1 shows the DTC switching table of a PMSM motor, where binary 1 and 0 indicate the ON and OFF states, respectively.

2.2 Golden eagle optimization (GEO)

The suggested arithmetical methodology for pretending the gestures of golden eagles chasing for target is labelled here. GE consumes the selection of circling its fi memory; therefore, $f \in \{1, 2\ldots, PopSize\}$. GE attack vector possibly will be projected by Eq. (9).

$$\overrightarrow{\mathrm{A_i}} = \overrightarrow{\mathrm{X_f}} - \overrightarrow{\mathrm{X_i}} \tag{9}$$

where eagle i attack vector is stated as $\overrightarrow{\mathrm{A_i}}$; best position is signified as $\overrightarrow{\mathrm{X_f}}$; present position is stated as $\overrightarrow{\mathrm{X_i}}$. Eq. (10) discovers the fixed variable value.

$$c_k = \frac{d-\sum_{jj\neq k} a_j}{a_k} \tag{10}$$

where c_k is destination point $c\ of\ k^{th}$ element, a_j is the j^{th} element of attack vector $\overrightarrow{A_i}$, The attack vector is signified as a_k^t, and fixed variable's index is stated as k. The cruise hyperplane's random endpoint is discovered in Eqs. (11) and (12).

$$\overrightarrow{C_i} = \left(c_1 = random, c_2 = random, \ldots c_k = \frac{d-\sum_{jj\neq k} a_j}{a_k}, \ldots, c_n = random\right) \tag{11}$$

$$\Delta x_i = \overrightarrow{r_1} P_a \frac{\overrightarrow{A_i}}{\|\overrightarrow{A_i}\|} + \overrightarrow{r_2} P_c \frac{\overrightarrow{C_i}}{\|\overrightarrow{C_i}\|} \tag{12}$$

where, attack & cruise coefficient in iteration t is signified as p_a^t and p_c^t. The random vectors $\overrightarrow{r_1}$ and $\overrightarrow{r_2}$ have elements that are in the duration [0 1]. Later, P_a and P_c can be deliberated. The Euclidean norms of the attack and cruise vectors ($\|\overrightarrow{A_i}\|$ and $\|\overrightarrow{C_i}\|$) are determined using Eq. (13).

$$\|\overrightarrow{A_i}\| = \sqrt{\sum_{j=1}^{n} a_j^2}, \|\overrightarrow{C_i}\| = \sqrt{\sum_{j=1}^{n} c_j^2} \tag{13}$$

The GE position is represented as Eq. (14).

$$x^{t+1} = x^t + \Delta x_i^t \tag{14}$$

The attack coefficient P_a^t and the cruise coefficient P_c^t determine the step vector which is impacted by cruise and attack vectors, respectively. GEO employs $p_a\ and\ p_c\ as$ the transition from exploration to exploitation. Low p_a and high p_c are the starting points for the algorithm. p_a Steadily increases whereas p_c gradually decreases as the iterations progress. The linear transition used to calculate intermediate values which is expressed in Eq. (15).

$$\begin{cases} P_a = P_a^0 + \frac{t}{T}|P_a^t - P_a^0| \\ P_c = P_c^0 + \frac{t}{T}|P_c^t - P_c^0| \end{cases} \tag{15}$$

where t denotes the current iteration, T denotes the maximum iterations, P_c^0 and P_c^T denote the starting and absolute standards for susceptibility to attack (p_a), correspondingly.

2.3 ANFIS controller

ANFIS is a method that uses a combination of ANN and Fuzzy logic. To optimize the response in fuzzy systems, the rule base and membership functions must be manually created. As a result, calibrating a fuzzy logic system is a time-consuming process, so it cannot produce the desired results. The fuzzy logic is used to generate the basic ANFIS structure, which is then developed by the neural network. The Sugeno paradigm of ANFIS is employed in this paper, along with four rules. The

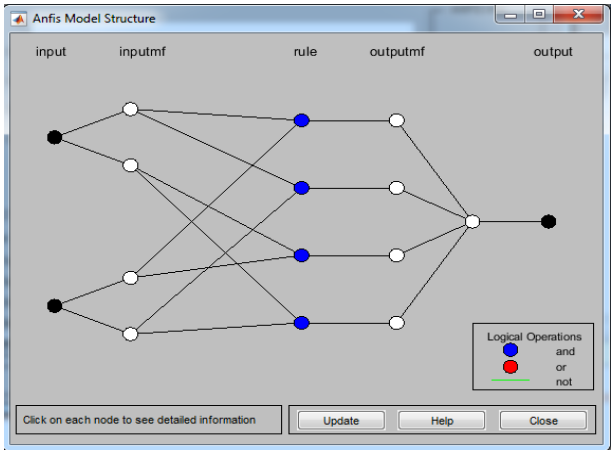

Figure. 3 Structure of ANFIS

ANFIS-based speed regulator has two variable inputs: speed error and change in error.

The torque reference is the system's output, which is fed into the DTC. Fig. 3 displays the arrangement of the ANFIS-based reference torque estimator. Using ANFIS, the torque reference is constructed each time from the speed error (N*-N) and changes in speed error. The network has 20 nodes and has been trained for 12 epochs. The tuning of ANFIS is done using the grid partitioning method. In the system, the learned model replaces the PID controller. The equations of the speed error (N*-N) and the variation in speed error are auto-tuned, resulting in an excellent performance. The I/O data sets of the given system are the data set necessary for ANFIS learning training. ANFIS structure is divided into five layers, which is described as follows:

1st layer: It's the input layer, and it's made up of input variables. Every node in this layer analyses triangular/Gaussian/Two-Gaussian membership functions, and input variables are sent to the next layer.

Layer 2: This layer is identified as the membership function (MF) layer, and it allows you to check loads of every MF. In each iterative count, the non-linear factor a_{ij}, b_{ij}, c_{ij} of the input MF is updated through the subsequent Eq. (16)

$$a_{ij}{}^{(1)}(n+1) = \alpha\left(a_{ij}{}^{(1)}(n)\right) + \eta\left(-\frac{\partial E(n)}{\partial a_{ij}{}^{(1)}}\right)$$

$$b_{ij}{}^{(1)}(n+1) = \alpha\left(b_{ij}{}^{(1)}(n)\right) + \eta\left(-\frac{\partial E(n)}{\partial b_{ij}{}^{(1)}}\right)$$

$$c_{ij}{}^{(1)}(n+1) = \alpha\left(c_{ij}{}^{(1)}(n)\right) + \eta\left(-\frac{\partial E(n)}{\partial c_{ij}{}^{(1)}}\right) \quad (16)$$

η is referred as learning rate; n is signified as step time; α is stated as steepest descent momentum constant.

Layer 3: In this layer, each neuron fulfils the necessary conditions of fuzzy rules. The network structure is equal to the fuzzy procedures count, and each node of these layers estimates the normalized weights. It's acknowledged using the rule layer.

Layer 4: Also recognized using defuzzification layer; it creates output values based on the application of rules. The fuzzy singletons that characterize an additional set of conditions for the neuro-fuzzy network are used to weight links between layers 3 and 4.

Layer 5: It collects all of the defuzzification layer's deliverables and turns the fuzzy sets to a crisp value and this layer is known as the output layer.

2.4 GEO optimized ANFIS

GEO optimized Learning parameter (η and α) for ANFIS over various working circumstances of PMSM drive are discussed here. In order to guarantee constancy and accomplish higher restraining to unexpected load disruption and speed dissimilarities, the constraints possibly will be selected to reduce the subsequent objective function labelled by Eq. (17) which is deliberated as fitness function for the optimization.

$$J_1(S) = H_1 + H_2 \quad (17)$$

$$H_1 = \sqrt{\frac{\sum_m^{i=1}(\omega_{ref} - \omega_{act_i})^2}{m}}$$

$$H_2 = \begin{cases} \omega_{max} - \omega_{ref} & if\ \omega_{max} > \omega_{ref} \\ 0 & Otherwise \end{cases}$$

Maximum speed is signified as ω_{max}; Actual speed is stated as ω_{act_i}; reference speed is declared as ω_{ref}; Sample count is referred as m; the tuning parameters range is specified in below Eqs. (18) and (19),

$$0 \leq \eta \leq 2 \quad (18)$$

$$0 \leq \alpha \leq 2 \quad (19)$$

3. Simulation results and discussions

The outcomes of this research were validated using MATLAB software. MATLAB R2018a is used to implement and simulate GEO-ANFIS which runs on a Windows 8 operating system with an Intel Core i3 processor and 4GB RAM. This paper discusses the speed management of a PMSM motor drive that is controlled using the DTC technique. GEO-ANFIS controller is simple to create and install because the

Received: April 26, 2022. Revised: June 7, 2022.

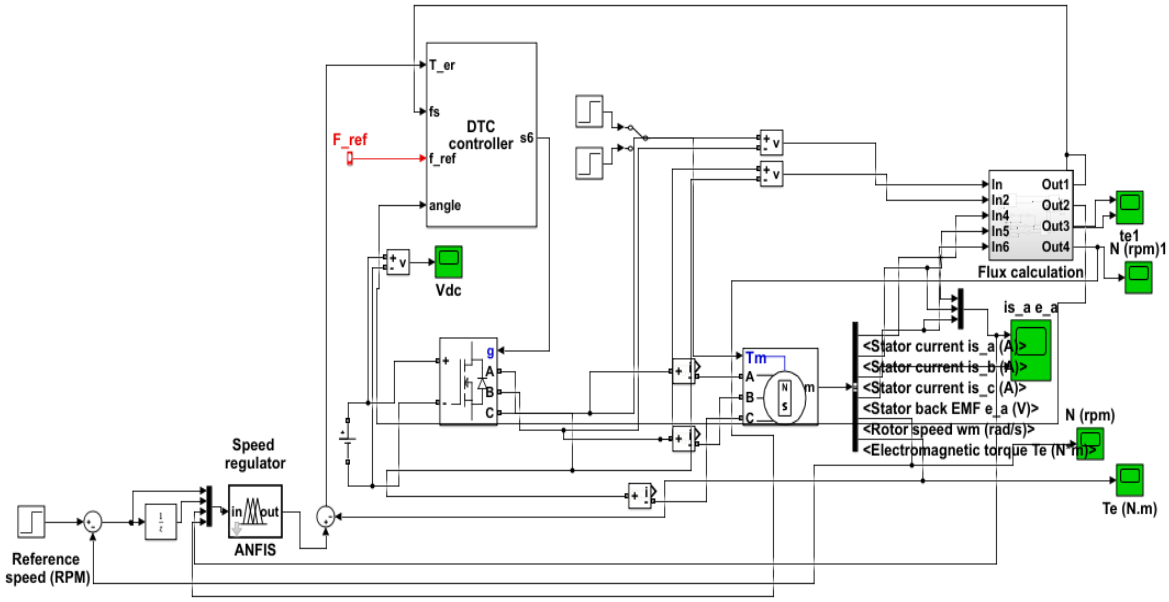

Figure. 4 DTC control of PMSM motor with GEO-ANFIS controller

Table 2. Specification of PMSM motor

PARAMETERS	VALUES
Weighting factor	1
Viscous friction	0.0017 kgm/s^2
Stator Resistance	0.636 ohm
Rated current	11.36A
Rated speed	4000 rpm
Rated torque	1.8 Nm
q-axis inductance	0.02H
PM motor Flux	0.088Wb
Number of Pole Pairs	2
Moment of inertia	0.0017 kgm^2
d-axis inductance	0.012H

equation and rule libraries are robust. Torque is calculated in the rotating dq - reference frame in this approach. Based on the simulation results, this method can be employed for high-performance applications. Modifications in the load can also help to improve dynamic performance. Because the drivetrain is sensitive to resistance changes, parameter adaptation can be used to boost performance even more. MATLAB simulation tools are used to execute the DTC of PMSM motor.

Speed, current, and flux graphs are used to assess the ability. Fig. 4 shows how to use MATLAB/Simulink to create DTC control of a PMSM motor using GEO-ANFIS. The entire Simulink model control variables can be found in Table 2. The sample rate is set to 50 seconds. The hysteresis bands are tuned at 1.8 N.m and 0.088 Wb, individually. As shown in Fig. 4, the stator flux and electromagnetic torque can be computed using stator current and input voltage. The speed of the motor is used as feedback, and the speed inaccuracy is

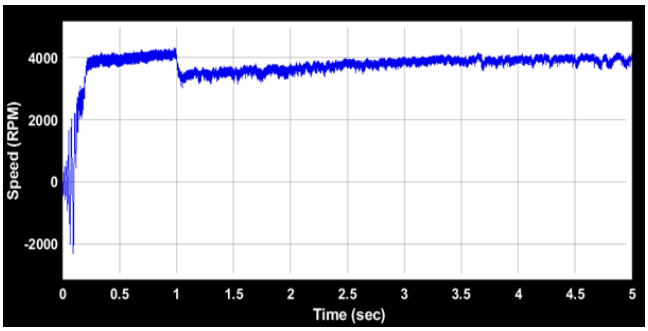

Figure. 5 Speed regulation for ANFIS controller

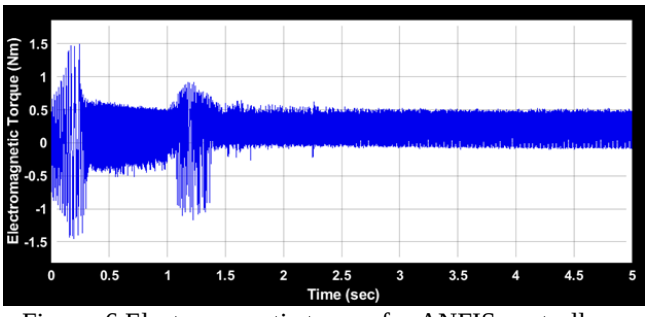

Figure. 6 Electromagnetic torque for ANFIS controller

calculated by comparing it to the reference speed. The GEO-ANFIS controller is given the anticipated speed error, variation as well as reference value of 4000. The GEO-ANFIS controller calculates the torque reference, which is related to the definite electromagnetic torque of the PMSM motor. The flux and torque are utilized to control the inverter's switching pattern. The entire simulation takes two seconds to finish. The induced load torque is 0.2Nm, and the load torque is sustained for one second. The PMSM motor's specifications are listed in Table 3. The speed and torque of the PMSM are shown in Fig. 5 to 7 depict the PMSM Motor's stator current.

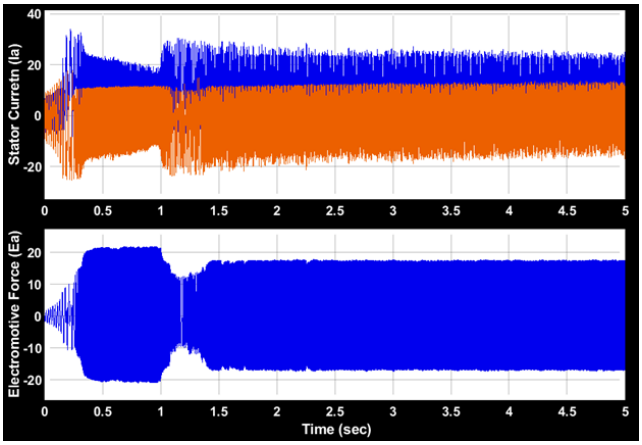

Figure. 7 EMF and current waveforms for ANFIS

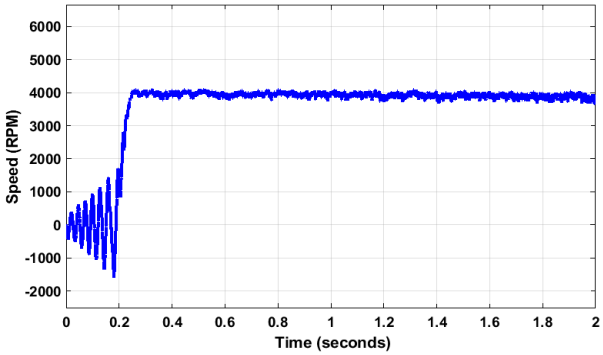

Figure. 8 Speed regulation for GEO-ANFIS controller

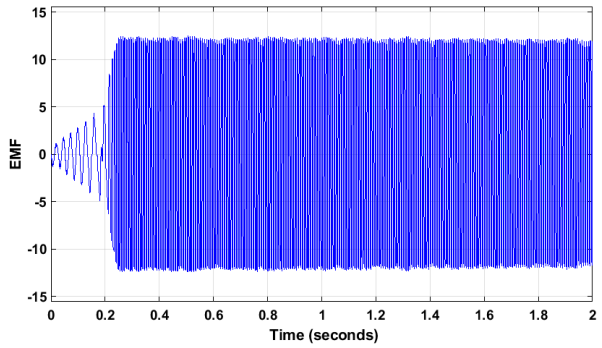

Figure. 9 EMF waveform for GEO-ANFIS controller

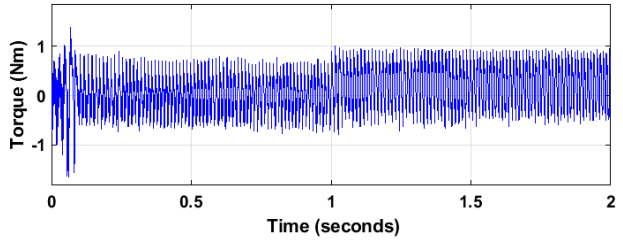

Figure. 10 Electromagnetic torque for GEO-ANFIS controller

When compared to the ANFIS controller, the results reveal that GEO-ANFIS produces better outcomes. It also has the potential to improve the system's stability. The existing PID and ANFIS controllers achieve a steady-state in 3.5 and 2.5 seconds, respectively. The proposed GEO-ANFIS achieved a stable state at 2.1 seconds which is better than existing controllers.

Table 3. Comparison for steady state performance of PMSM motor

Parameters	PID Controller	ANFIS	GEO-ANFIS
Steady State Comparison	3.5 sec	2.1 sec	1.9 sec

Table 4. Comparison for transient response of PMSM motor

Constraints	HGA-GSA [17]	ANFIS	GEO-ANFIS
Settling Time (sec)	0.89	0.19	0.12
Rising time (sec)	0.04	0.05	0.03
Overshoot time (%)	-	6.04	5.59

The results of the steady state comparison are exposed in Table 3. The steady state analysis are implemented with existing PID, ANFIS and proposed GEO optimized ANFIS controller Fig. 8, 9 and 10 show the speed, EMF and torque results of the GEO-ANFIS controller.

Table 4 shows the comparative analysis of transient responses with existing HGA-GSA [17] and ANFIS controller. Even if the ANFIS have better results in the settling times, but the overshoot is much more noticeable which destroys the other transitory performance criteria. From the Table 4, it clearly shows that proposed GEO-ANFIS achieved better transient performance than existing HGA-GSA [17] and ANFIS. Table 5 clearly illustrates that the recommended GEO-ANFIS outperforms the conventional controllers in terms of settling time, rising time and overshoot time. Fig. 11 and 12 shows the transient performance of Speed and Torque using the GEO-ANFIS controller.

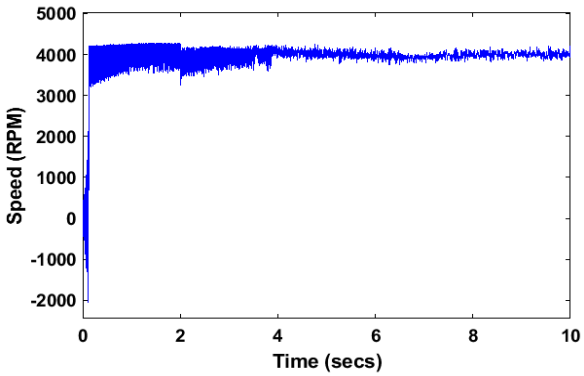

Figure. 11 Transient response of speed for GEO-ANFIS controller

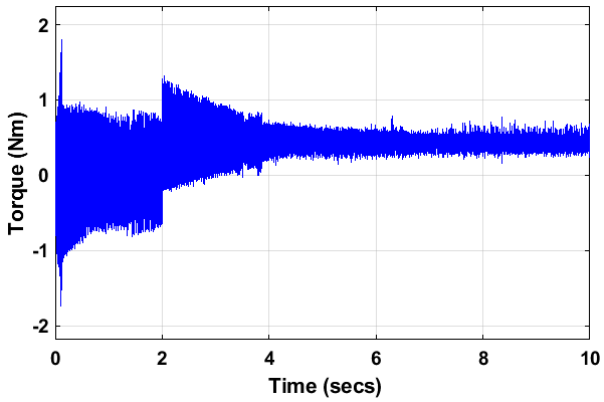

Figure. 12 Transient response of torque for GEO-ANFIS controller

Table 5. Comparison for torque ripple

Parameters	HWOA [16]	SVPWM-DTC [21]	ANFIS	GEO-ANFIS
Torque Ripple (Nm)	1.62	0.60	0.53	0.44

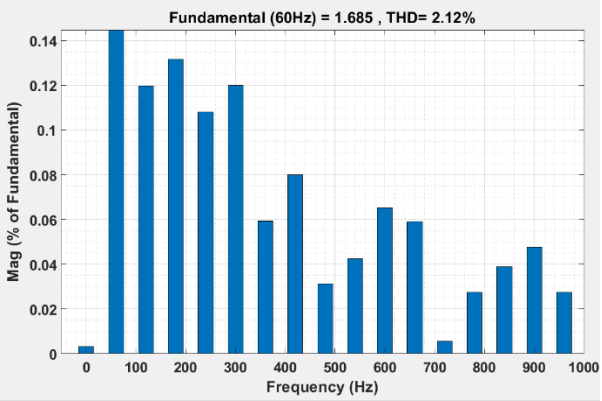

Figure. 13 FFT analysis

Table 5 shows the comparison of torque ripple. From Table 5, it clearly shows that the proposed GEO-ANFIS achieves less torque ripple over the existing HWOA [16], SVPWM-DTC [21] and ANFIS. The number of pole pairs in a mechanical motor with a speed of 2000 rpm is 3, and 12th harmonics frequency is 1.2 kHz. The proposed GEO-ANFIS achieves less torque ripple of 0.44 Nm, which is better than the existing HWOA [16], SVPWM-DTC [21] and ANFIS which attained 1.62, 0.60 and 0.53 Nm respectively.

Fig. 13 shows the FFT analysis of the PMSM motor. Where Table 6 shows the comparative analysis of Total Harmonic Distortion. The control approach with the suggested GEO-ANFIS controller outperforms the existing DCF-MPDSC [22] and ANFIS controller.

From the Fig. 13, it clearly shows that the proposed GEO optimized ANFIS achieves a better

Table 6. Comparison for THD

Parameters	DCF-MPDSC [22]	ANFIS	GEO-ANFIS
THD (%)	4.43	2.33	2.12

THD of 2.12 % which is less when compared with existing ANFIS and DCF-MPDSC [22] which accomplishes 2.33% and 4.43% respectively.

4. Conclusion

This research presented the DTC of PMSM by GEO optimized ANFIS Controller. Learning factors of ANFIS are optimized by means of GEO under various conditions. GEO-ANFIS speed controller is used to achieve closed loop operation. By exchanging the speed regulator with a conventional PID and GEO-ANFIS controller, the DTC control of a PMSM motor with its dynamic qualities has been improved. In the conventional SVPWM-DTC & DCF-MPDSC controller, it takes an extended time to reach a stable state and the time delay is minimized by the proposed GEO-ANFIS controller. From the MATLAB/Simulink, it evidently shows that the proposed GEO-ANFIS is capable to remove the improbability issues happening because of speed/load fluctuations. The results reveal that the proposed approach provides less torque ripple of 0.44 Nm and provides less THD of 2.12% which improves system performance when compared with DCF-MPDSC Controller. In the future, this research work can be extended with different optimization techniques or hybrid intelligent techniques.

Conflicts of Interest

The authors declare no conflict of interest.

Author Contributions

The paper conceptualization, methodology, software, validation, formal analysis, investigation, resources, data curation, writing—original draft preparation, writing—review and editing, visualization, have been done by 1st author. The supervision and project administration, have been done by 2nd author.

References

[1] M. Sellali, A. Betka, S. Drid, A. Djerdir, L. Allaoui, and M. Tiar, "Novel control implementation for electric vehicles based on fuzzy-back stepping approach", *Energy*, Vol. 178, pp. 644-655, 2019.

[2] T. Liu, G. Chen, and S. Li, "Application of vector control technology for PMSM used in

electric vehicles", *The Open Automation and Control Systems Journal*, Vol. 6, No. 1, 2014.

[3] X. Sun, Z. Li, X. Wang, and C. Li, "Technology development of electric vehicles: A review", *Energies*, Vol. 13, No. 1, 2020.

[4] Y. Yang, Q. He, C. Fu, S. Liao, and P. Tan, "Efficiency improvement of permanent magnet synchronous motor for electric vehicles", *Energy*, Vol. 213, p. 118859, 2020.

[5] S. Gao, Y. Wei, D. Zhang, H. Qi, and Y. Wei, "A modified model predictive torque control with parameters robustness improvement for PMSM of electric vehicles", *Actuators*, Vol. 10, No. 6, p. 132, 2021.

[6] H. Elsherbiny, M. Ahmed, and M. Elwany, "Comparative evaluation for torque control strategies of interior permanent magnet synchronous motor for electric vehicles", *Periodica Polytechnica Electrical Engineering and Computer Science*, Vol. 65, No. 3, pp. 244-261, 2021.

[7] D. Kumpanya, D. S. Thaiparnat, and D. Puangdownreong, "Parameter identification of PMSM motor model via metaheuristic optimization techniques", *Procedia Manufacturing*, Vol. 4, pp. 322-327, 2015.

[8] K. Hartani, A. Merah, and A. Draou, "Stability enhancement of four-in-wheel motor-driven electric vehicles using an electric differential system", *Journal of Power Electronics*, Vol. 15, No. 5, pp. 1244-1255, 2015.

[9] X. Qiu, W. Huang, and F. Bu, "Torque-angle-based direct torque control for interior permanent-magnet synchronous motor drivers in electric vehicles", *Journal of Power Electronics*, Vol. 13, No. 6, pp. 964-974, 2013.

[10] R. Babu and B. M. Kumar, "Comparative Analysis of PMSM motor for different control topology", *Energy Procedia*, Vol. 117, pp. 314-320, 2017.

[11] H. Mesloub, R. Boumaaraf, M. T. Benchouia, A. Goléa, N. Goléa, and K. Srairi, "Comparative study of conventional DTC and DTC_SVM based control of PMSM motor—Simulation and experimental results", *Mathematics and Computers in Simulation*, Vol. 167, pp. 296-307, 2020.

[12] M. Abhishek, R. S. Wahab, G. C. S. Reddy, C. Annamalai, and U. Subramaniam, "Assessing Finite Control Set Model Predictive Speed Controlled PMSM Performance for Deployment in Electric Vehicles", *World Electric Vehicle Journal*, Vol. 12, No. 1, 2021.

[13] V. Pushparajesh, B. M. Nandish, and H. B. Marulasiddappa, "Hybrid intelligent controller based torque ripple minimization in switched reluctance motor drive", *Bulletin of Electrical Engineering and Informatics*, Vol. 10, No. 3, pp. 1193-1203, 2021.

[14] A. Ghamri, R. Boumaaraf, M. T. Benchouia, H. Mesloub, A. Goléa, and N. Goléa, "Comparative study of ANN DTC and conventional DTC controlled PMSM motor", *Mathematics and Computers in Simulation*, Vol. 167, pp. 219-230, 2020.

[15] M. Abassi, O. Khlaief, O. Saadaoui, A. Chaari, and M. Boussak, "Real-time implementation of discrete Fourier transform phase analysis and fault tolerant control for PMSM in electric vehicles", *COMPEL-The International Journal for Computation and Mathematics in Electrical and Electronic Engineering*, 2018.

[16] Z. Jin, X. Sun, G. Lei, Y. Guo, and J. Zhu, "Sliding mode direct torque control of SPMSMs based on a hybrid wolf optimization algorithm", *IEEE Transactions on Industrial Electronics*, Vol. 69, No. 5, pp. 4534-4544, 2021.

[17] S. Ünsal and I. Aliskan, "Investigation of performance of fuzzy logic controllers optimized with the hybrid genetic-gravitational search algorithm for PMSM speed control", *Automatika*, Vol. 63, No. 2, pp. 313-327, 2022.

[18] Z. Zhang and X. Liu, "A duty ratio control strategy to reduce both torque and flux ripples of DTC for permanent magnet synchronous machines", *IEEE Access*, Vol. 7, pp. 11820-11828, 2019.

[19] X. Wang, Z. Wang, and Z. Xu, "A hybrid direct torque control scheme for dual three-phase PMSM drives with improved operation performance", *IEEE Transactions on Power Electronics*, Vol. 34, No. 2, pp. 1622-1634, 2018.

[20] N. M. Javad, J. Milimonfared, and H. A. Talebi, "Torque and flux ripples minimization of permanent magnet synchronous motor by a predictive-based hybrid direct torque control", *IEEE Journal of Emerging and Selected Topics in Power Electronics*, Vol. 6, No. 4, pp. 1662-1670, 2018.

[21] Z. Zhong, J. You, and S. Zhou, "Torque Ripple Reduction of DTC Based on an Analytical Model of PMSM", *World Electric Vehicle Journal*, Vol. 11, No. 1, p. 28, 2020.

[22] M. Liu, J. Hu, K. W. Chan, S. W. Or, S. L. Ho, W. Xu, and X. Zhang, "Dual cost function model predictive direct speed control with duty ratio optimization for PMSM drives", *IEEE Access*, Vol. 8, pp. 126637-126647, 2020.

[23] H. B. Marulasiddappa and V. Pushparajesh, "Review on different control techniques for

induction motor drive in electric vehicle", In: *Proc. of IOP Conference Series: Materials Science and Engineering*, Vol. 1055, No. 1, pp. 012142, 2021.

Notations

Notation	Description
V_a, V_b and V_c	Stator Phase Voltages
E_a, E_b and E_c	Trapezoidal Back EMF
i_a, i_b and i_c	Motor Input Current
R_a, R_b and R_c	Terminal Resistances
L	Self-Inductances
M	Mutual inductances
T_e	Electromagnetic Torque
p_n	Number of Poles
i_{sd}, i_{sq}	Current at d and q axes
L_d and L_q	Inductances at d and q axes
θ_r	Rotor Angle
φ_{rd}, φ_{rq}	Rotor Flux
φ_{sd}, φ_{sq}	Stator Flux
$\varphi_{r\alpha}$ and $\varphi_{r\beta}$	Rotor Flux Linkage
$\varphi_{s\alpha}(0)$ and $\varphi_{s\beta}(0)$	Initial Stator flux linkage
K_b	Back EMF Constant
fi	Circle Selection
$\overrightarrow{\mathrm{A}_1}$	Attack vector
$\overrightarrow{\mathrm{X}_\mathrm{f}}$	Best position
$\overrightarrow{\mathrm{X}_1}$	Current position
c_k	Destination point
k	Fixed variable index
p_a^t	Attack coefficient
p_c^t	Cruise coefficient
ω_{ref}	Reference speed
$\overrightarrow{r_1}$ and $\overrightarrow{r_2}$	Random vectors
$\|\overrightarrow{A_i}\|$ and $\|\overrightarrow{C_i}\|$)	Euclidean norms of attack and cruise vectors
t	Current iteration
T	Maximum iteration
n	Step time
ω_{max}	Maximum speed
η	Learning rate
α	Steepest descent momentum constant
m	Sample count